OPEN DOCUMENT - PROJECT REPORT

THE MAPPING OF TEXTURE FUNCTIONS ON FINITE ELEMENT GRIDS FOR ANISOTROPY SIMULATIONS

D. Raabe

Max-Planck-Institut für Eisenforschung
Max-Planck-Str. 1
40237 Düsseldorf
Germany

January 2004, Max-Planck-Society
http://www.mpg.de *http://www.mpie.de* *http://edoc.mpg.de*

Keywords orientation distribution function, simulation, crystallographic texture, crystal plasticity, anisotropy, finite elements

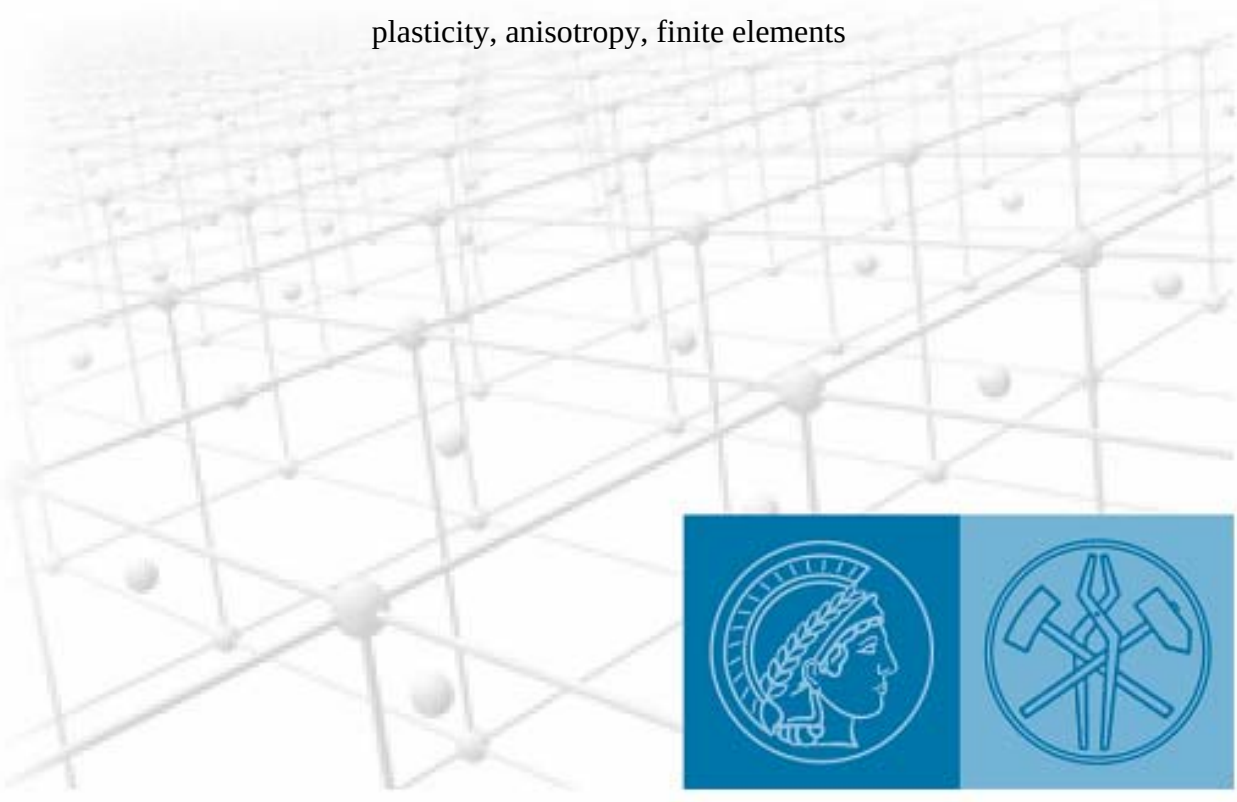

Project References

D. Raabe, M. Sachtleber, Z. Zhao, F. Roters, S. Zaefferer: Acta Materialia 49 (2001) 3433–3441

„Micromechanical and macromechanical effects in grain scale polycrystal plasticity experimentation and simulation”

D. Raabe, Z. Zhao, S.–J. Park, F. Roters: Acta Materialia 50 (2002) 421–440

„Theory of orientation gradients in plastically strained crystals”

Z. Zhao, F. Roters, W. Mao, D. Raabe: Adv. Eng. Mater. 3 (2001) p.984/990

„Introduction of A Texture Component Crystal Plasticity Finite Element Method for Industry-Scale Anisotropy Simulations”

M. Sachtleber, Z. Zhao, D. Raabe: Materials Science and Engineering A 336 (2002) 81–87, “Experimental investigation of plastic grain interaction”

D. Raabe, P. Klose, B. Engl, K.-P. Imlau, F. Friedel, F. Roters: Advanced Engineering Materials 4 (2002) 169-180

„Concepts for integrating plastic anisotropy into metal forming simulations”

D. Raabe, Z. Zhao, W. Mao: Acta Materialia 50 (2002) 4379–4394

„On the dependence of in-grain subdivision and deformation texture of aluminium on grain interaction”

D. Raabe: Annual Review of Materials Research 32 (2002) p. 53-76

„Cellular automata in materials science with particular reference to recrystallization simulation”

D. Raabe: Advanced Materials 14 No. 9 (2002) p. 639-650

„Challenges in Computational Materials Science”

D. Raabe and F. Roters: International Journal of Plasticity 20 (2004) p. 339-361

„Using texture components in crystal plasticity finite element simulations”

D. Raabe, M. Sachtleber, H. Weiland, G. Scheele, and Z. Zhao: Acta Materialia 51 (2003) 1539-1560.

„Grain-scale micromechanics of polycrystal surfaces during plastic straining”

S. Zaefferer, J.-C. Kuo, Z. Zhao, M. Winning, D. Raabe: Acta Materialia 51 (2003) 4719-4735.

„On the influence of the grain boundary misorientation on the plastic deformation of aluminum bicrystals”

Project Abstract

The study discusses how crystal orientation distributions can be mapped on finite element grids for conducting large scale anisotropy simulations which use anisotropic crystalline constitutive laws. Methods based on direct pole figure inversion, series expansions of spherical harmonics, or a large sets of discrete orientation values are not appropriate to reproduce crystallographic textures in a sufficiently localized spherical form onto finite element grids. The texture component method which employs Lorentz or Gauss shaped spherical functions is better suited for this task. It offers a good compromise between discreteness (spherical localization), exactness (approximation of complicated orientation distribution functions can be achieved by a few texture components), compactness (simple functions), scalability (the number of used texture components can be systematically varied according to the desired precision of the texture fit), and physical significance (texture components are related to microstructural mechanisms).

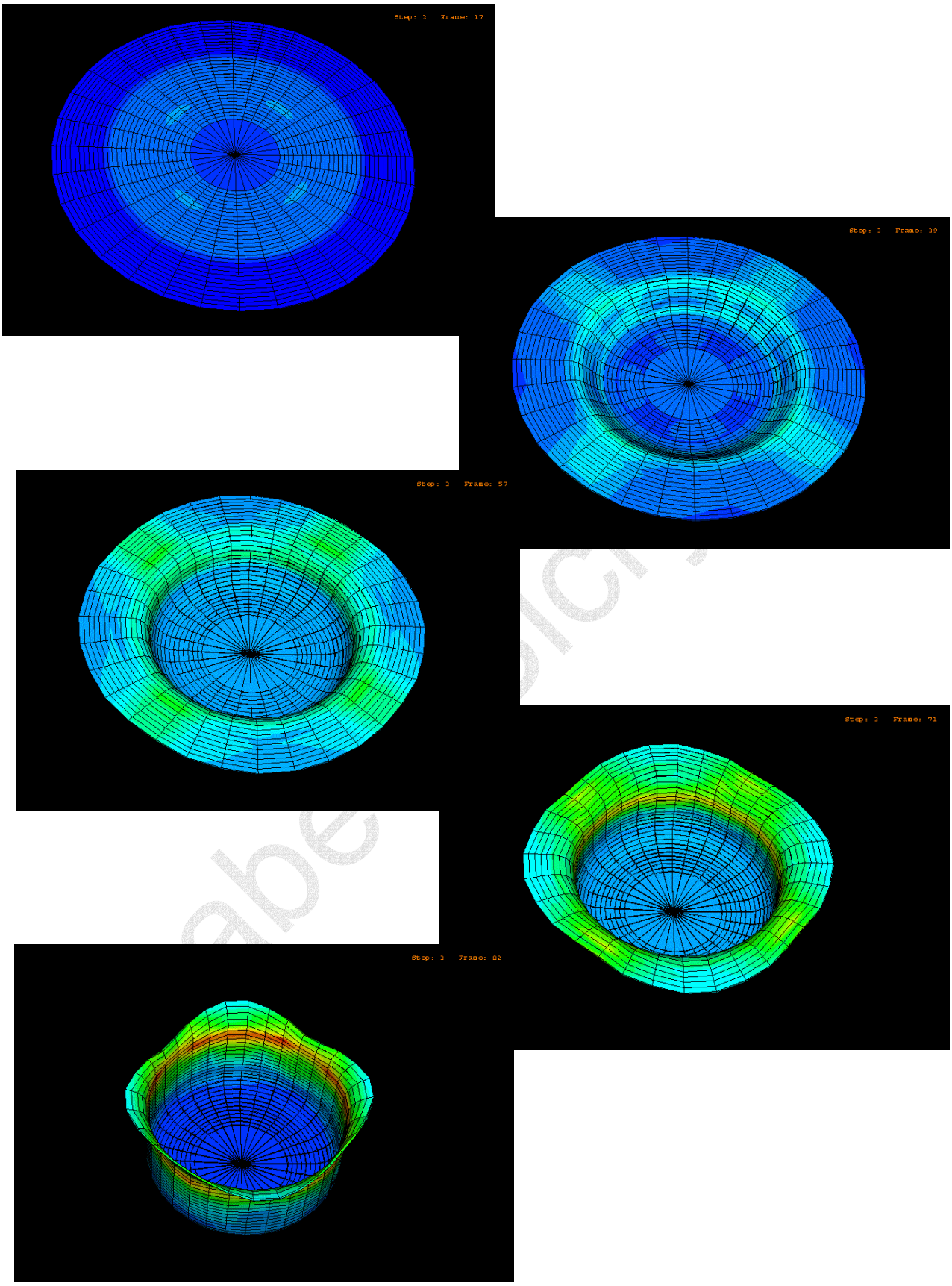
Step: 3 Frame: 17
Step: 3 Frame: 29
Step: 3 Frame: 57
Step: 3 Frame: 71
Step: 3 Frame: 82

1 Introduction

Modern experimental and theoretical methods for investigating crystallographic orientation distributions (textures) facilitate and in part necessarily entail the accumulation of data sets consisting of huge sets of discrete crystallographic orientation values (microtexture, nanotexture) or pole figure projections of statistical orientation distributions (macrotexture). In either case quantitative standard measures must be identified to utilize these data in subsequent polycrystal anisotropy simulations which incorporate orientation dependent constitutive laws.

Examples are the mapping of crystallographic textures into mathematical methods for predictions of elastic and elastic-plastic anisotropy, ferromagnetic response, thermal expansion, and the resistive electrical conductivity of textured polycrystalline matter containing large numbers of crystals and its integral response to mechanical and/or electromagnetical loadings. The second even more demanding task along this line is the prediction of the *change* of crystalline anisotropy during loading, as for instance occurring during elastic-plastic deformation where the crystals individually rotate and subdevide during deformation owing to the antisymmetry of the displacement gradients created by crystal slip.

This study deals with the integration of crystallographic texture data into such large scale anisotropy simulations. Particular pronunciation is placed on reducing redundant texture information to a level where sufficient details can be recovered without loosing physical significance.

This rather complex problem can be split into two quite separate tasks (Figure 1 [1]). The first one is the formulation of a basic solution method which uses texture as a state variable. This is typically achieved by formulating an orientation dependent constitutive law which maps the requested physical anisotropy at the single crystal scale and by embedding this formulation into a finite element code. The numerical implementation then tackles the interaction of the differently oriented volume portions and thereby predicts the integral response of the sample under loads. Any such formulation requires a *discrete* representation of the orientation distribution function or a portion of it at each integration point. Therefore, the second task consists in mapping *single* orientations directly on the Gauss points of the finite element mesh or in decomposing orientation distributions in such a way that they can be subsequently mapped on a mesh in a manner that they correspond to the initial overall distribution.

Integral anisotropy predictions of polycrystalline matter can in principle be conducted by directly feeding sets of discrete orientations onto the integration points of finite element models, i.e. by simply assigning each orientation to a separate integration point. However, such a mapping method is not practicable when aiming at the simulation of specimens which consist for instance of 10^{10} discrete crystals. A second limitation comes from the necessity to formulate a *scalable* method. Scalability in this context means the requirement to map large as well as small texture data sets with equal mathematical consistency. Both aspects suggest the introduction of a compact mathematical form to map and update textures properly in anisotropy predictions. The present study discusses the advantages and disadvantages of some functions available for the representation of textures under the special boundary conditions mentioned above. This means in particular the requirement for a *discrete* representation of the orientation distribution function or a portion of it at each integration point.

2 Basic approaches for the reproduction of the orientation distribution function

2.1 Introduction

The orientation distribution of the crystals assembling a polycrystalline aggregate, *f(g)*, can be reproduced from two-dimensional centro-symmetric projections which are referred to as pole figures or sets of single orientations [2-5]. In either case different mathematical methods can be used. In the first case the orientation distribution is commonly described in terms of the direct inversion of the pole figures or in terms of Fourier-based series expansion methods which use spherical harmonics as library functions. In the second case one commonly reproduces the orientation distribution by use of large sets of discrete single grain orientations with identical scatter and amplitude or by use of the texture component method where each preferred orientation has *individual* scatter and amplitude.

2.2 Series expansion methods

In the Fourier-type series expansion methods the orientation distribution function is approximated by computing the coefficients $C_l^{\mu\nu}$ of its orthogonal expansion from the expansion coefficients $F_l^{\nu}(h_i)$ of experimentally detected pole figures [2-5]. Since the centro-symmetric pole figures are expanded with a series of even order spherical harmonics, only the even order coefficients $C_l^{\mu\nu}$ of $f(g)$ are generated, rendering the so determined function an approximate orientation distribution function containing only the even part of $f(g)$ which is referred to as $\tilde{f}(g)$. The complete function, $f(g)$, is named true orientation distribution function. The real orientation distribution is hence given by the equation $f(g) = \tilde{f}(g) + \tilde{\tilde{f}}(g)$, where $\tilde{\tilde{f}}(g)$ represents any function which can be added to $\tilde{f}(g)$ without changing corresponding projections, i.e. pole figures [6]. The even function $\tilde{f}(g)$ usually causes texture dependent errors which are referred to ghost components. They can lead to positive or negative deviations from the true orientation distribution function. For reducing ghost intensities in the orientation distribution function advanced series expansion methods use the non-negativity condition which led to the development of an iterative series-expansion method [5, 7-9].

2.3 Direct pole figure inversion

The methods which use direct inversions of pole figure projections were formulated by Williams [10], Ruer and Baro [11], Imhof [12], Matthies and Vinel [13], and Pawlik [14]. They approximate textures in terms of the direct integration of the fundamental equation of texture analysis using a set of experimental pole figures. Since the direct inversion methods directly use the discrete form of the fundamental equation for pole figure inversion they work in real space and not in Fourier space. This means that these approaches make use of the fact,

that the discrete hemisphere of the pole figure corresponds to families of projection tubes in the $f(g)$ space, i.e. the non-negativity condition for the orientation distribution function is automatically taken into account. The solution is achieved by iteration. The direct methods are – like all texture reproduction methods which use starting data of higher symmetry (i.e. 2D projections) than the orientation distribution function – affected by the inversion symmetry of the pole figure data entailing positive or negative texture portions without physical significance (texture ghosts) [5,14-16]. In the discrete form, cells in the pole figures and in the $f(g)$ space are directly related by linear equations. The density in each pole figure cell is the sum of the corresponding cell densities in the $f(g)$ space. Since different $f(g)$ sums lead to the same pole density, the set of linear equations is underdetermined which leads to so called ghost errors in the orientation distribution function. The second disadvantage of the direct inversion methods is that they do not provide Fourier coefficients. Although this shortcoming is inevitably connected with all direct approaches it can be avoided by subsequently fitting an orientation distribution function derived by direct inversion using a series expansion or a texture component based method (for the latter approach see next section). Fourier coefficients of texture functions are generally desirable because they facilitate the calculation of anisotropic behavior such as directional elastic, magnetic, or electrical properties of polycrystalline aggregates from texture data. Although directional physical properties are of course not necessarily connected to Fourier coefficients, their employment permits high speed calculations of integral properties of textured samples particularly in cases where homogenization theory is used to couple texture and properties.

2.4 Texture component methods

Mapping discrete portions of a statistical orientation distribution requires the reduction of the information content to a level at which complex integral anisotropy problems arising from the interaction of large numbers of intrinsically anisotropic crystals can be simulated at reasonable computation costs. Such an approach is provided by the texture component method [17-22]. It goes back to the early texture studies where experimental and predicted pole figures were mostly interpreted in terms of the evolution and physical significance of single discrete texture components [23]. Classical terms introduced in these early studies on crystallographic orientation distributions were for instance the “Copper texture component”, the “Brass texture component”, and the “Taylor texture component”. The use of preferred orientations prevailed in texture research until the late sixties of the last century, i.e. statements about texture evolution were made practically exclusively on the basis of pole figures and estimated preferred components (ideal positions, texture components). Modern approaches which describe texture components in orientation space [17-22] approximate the orientation distribution function by a superposition of sets of Gauss- or Lorentz-shaped model functions with individual height and individual full width at half maximum as a measure for the strength and scatter of a crystallographic texture component in orientation space. Such a discrete representation of a preferred orientation is referred to as a texture component. In contrast to the use of global symmetric Wigner functions for instance in the Fourier-type series expansion methods, the texture component method is based on using localized spherical normalized standard functions.

The described properties clearly qualify the texture component approach as a key method for directly extracting texture information in a compact fashion from experiment or theory and subsequently feeding it into finite-element based anisotropy simulations which involve large numbers of crystals. The following sections will give a concise mathematical review of the

texture component method and explain how texture components can be mapped on a finite element grid in cases where the underlying constitutive model has been formulated in an orientation dependent fashion [24-27].

3 Basic formulation of the texture component method

Following the work of Helming [20-22] the mathematical reproduction of the orientation distribution function by texture component functions which are locally restricted in orientation space can be expressed by the superposition

$$f(g) = F + \sum_{c=1}^{C} I^c f^c(g) = \sum_{c=0}^{C} I^c f^c(g) \quad \text{where} \quad I^0 = F,\ f^0(g) = 1 \tag{1}$$

where g is the orientation, $f(g)$ is the orientation distribution function and F is the volume portion of all randomly oriented crystals (random texture component). F may be understood as the intensity of the only *global* component used in the model, which is given by $f^c(g) = 1$ for each orientation point in Euler space, $g \in G$ .The intensity I^c describes the volume fraction of all crystallites belonging to the component c. Figure 2 shows a schematical sketch of a spherical texture component c which is described in terms of a maximum orientation density at a preferred orientation g^c and scatter width b^c. The orientation density of the component decreases with increasing orientation distance $\tilde{\omega}^c = \tilde{\omega}(g^c, g)$ from the maximum, i.e. $f^c(g)$ only depends on $\tilde{\omega}^c = \tilde{\omega}(g^c, g)$ and is independent on the rotation axis $\tilde{n}^c$.

The orientation distribution function is defined by

$$f(g)\,\mathrm{d}g = 8\pi^2 \frac{\mathrm{d}V_g}{V} \qquad \text{which implies} \qquad f(g) \geq 0 \tag{2}$$

where V is the sample volume and $\mathrm{d}V_g$ the volume of all crystals with an orientation g within the orientation portion $\mathrm{d}g = \sin(\phi)\,\mathrm{d}\phi\,\mathrm{d}\varphi_1\,\mathrm{d}\varphi_2$. Normalization requires

$$\oint f^c(g)\,\mathrm{d}g = 1 \qquad \text{which implies} \qquad \sum_{c=0}^{C} I^c = 1 \tag{3}$$

As a rule texture components require positivity, i.e.

$$f^c(g) \geq 0 \quad \text{for all} \quad g \in G \qquad \text{and} \qquad I^c > 0 \tag{4}$$

where G is the orientation space. Equation 4 can also be derived by using Equation 2 and the assumption that the texture components do not overlap in orientation space and that an orientation distribution function can be described by one single texture component.

Distribution functions which have a maximum at a preferred orientation g^c and decrease with increasing orientation distance $\tilde{\omega}^c = \tilde{\omega}(g^c, g)$ are referred to as central functions. Such functions, including corresponding pole figures, can be generally represented in the form of series expansions of χ functions or respectively Legendre polynomials. More practical approximations of texture components have been introduced on the basis of spherical Gauss- and Lorentz-functions. The examples presented later in this work made use of Gauss-shaped

model functions for the decomposition of the orientation distribution function which are described by

$$f^{c}(g) = N^{c} \exp\left(S^{c} \cos\tilde{\omega}\right) \tag{5}$$

where

$$S^{c} = \frac{\ln 2}{1-\cos(b^{c}/2)} \qquad \text{and} \qquad N^{c} = \frac{1}{I_0(S^{c}) - I_1(S^{c})} \tag{6}$$

and

$$P_h^M\left(g^{c}, b^{c}, y\right) = N^{c} \exp\left(S^{c} \sin(\upsilon^{c}/2)\right)\ I_0\left(S^{c} \cos(\upsilon^{c}/2)\right) \tag{7}$$

and

$$\cos\upsilon^{c} = h\left(g^{c}, y\right) \tag{8}$$

$I_l(x)$ are generalized Bessel functions. The value b^{c} is the halfwidth and can be interpreted as the mean diameter of a spherical component in orientation space [20-22].

Equation 7 shows that the corresponding pole figure projections $P_h^M\left(g^{c}, b^{c}, y\right)$ are given by closed analytical expressions. The components describing *f(g)* can be determined by the best fit of the experimental pole figure input data $\tilde{P}_{h_i}^M\left(y_r\right)/N_{h_i}$ with the recalculated pole figures $\sum_c I^{c} \tilde{P}_h^M\left(g^{c}, b^{c}, y_r\right)$. The index r marks the measured sample directions y_r. The component parameters I^{c}, g^{c} and b^{c} and the normalization N_{h_i} of the pole figures are obtained by solving the least squares problem

$$\sum_{i,r} w_{ir}\left[\tilde{P}_{h_i}\left(y_r\right)/N_{h_i} - \sum_c I^{c} \tilde{P}_{h_i}^M\left(g^{c}, b^{c}, y_r\right)\right]^2 \Rightarrow Min. \tag{9}$$

where w_{ir} are weight factors. Usually the parameters g^{c} and b^{c} must be calculated by a non-linear algorithm. First estimates are required, which may be obtained manually from the graphical representation of the difference pole figures which are calculated according to

$$\Delta_{h_i}\left(y_r\right) = \tilde{P}_{h_i}\left(y_r\right) - \sum_c I^{c} \tilde{P}_{h_i}^M\left(g^{c}, b^{c}, y_r\right) \tag{10}$$

Depending on experience in interpreting crystallographic textures the user can specify the position, height, and scatter of the texture components within certain bounds before the minimization. This makes particularly sense, when the number of texture components initially prescribed to match an experimental texture is small or when a certain scatter width of the components should not be exceeded. Further details on the method are given in the works of Helming et al. [20-22].

4 Main texture components for body centered and face centered cubic crystals

The texture component method provides a small set of compact functions which are characterized by simple parameters of physical significance (Euler angles, scatter, volume fraction). Usually, only a few texture components together with a random background component are required for representing textures in a precise mathematical form and for describing the integral anisotropy of a specimen.

The most important of these components in face centered cubic metals are the Cube-component ({001}<100>, φ_1=0°, ϕ=0°, φ_2=0°), the Goss-component ({011}<100>, φ_1=0°, ϕ=45°, φ_2=0°), the Brass-component ({0$\underline{1}$1}<211>, φ_1=35°, ϕ=45°, φ_2=0°), the Copper-component ({$\underline{2}$11}<111>, φ_1=90°, ϕ=35°, φ_2=45°), and the S-component (~{12$\underline{3}$}<634>, φ_1=60°, ϕ=32°, φ_2=65°).

In body centered cubic metals the most important texture components are the Rotated Cube component {001}<110> (φ_1=0°, ϕ=0°, φ_2=45°), the Inverse Brass-component {1$\underline{1}$2}<110> (φ_1=0°, ϕ=35°, φ_2=45°), the {1$\underline{1}$1}<110> component (φ_1=0°, ϕ=54.7°, φ_2=45°), the {111}<11$\underline{2}$> component (φ_1=30°, ϕ=54.7°, φ_2=45°), and the Goss-component ({011}<100>, φ_1=0°, ϕ=45°, φ_2=0°).

5 Mapping texture components onto discrete spatial grids

The main challenge of directly predicting integral polycrystal anisotropy on the basis of local single crystal behavior lies in identifying an efficient way of mapping an originally *statistical* and *representative* crystallographic orientation distribution in a *discrete* fashion on the integration points of a spatially discrete mesh (as for instance required for finite element implementation). This boundary condition favors the use of sets of localized spherical texture components.

Figure 3 explains how texture components can be embedded in discrete crystal anisotropy simulations. The example given in Figure 3a refers to a simulation of the integral elastic stiffness of a textured polycrystal. In this case the orientations are mapped as independent state variable on each Gauss point and the single crystal stiffness modulus acts as a constitutive law (see also Figure 1). The example given in Figure 3b refers to a simulation of the integral elastic-plastic response and the corresponding crystallographic reorientation rates of a textured polycrystal. In this case the orientations are also mapped as independent state variable on each Gauss point and the single crystal stiffness and slip systems including some plastic hardening rule act as constitutive laws.

Determination and mapping of the texture components proceeds as follows: In the first step the texture components must be recovered from experimental or theoretical data. This can be done by applying the texture component method formulated by Helming [20-22] as outlined in section 3. Mapping the components in a discrete fashion onto the integration points of a finite element mesh is conducted in two separate steps. First, the discrete preferred orientation (center orientation, mean orientation) of each texture component is equally assigned in terms of its respective Euler triple (φ_1, ϕ, φ_2) onto each of the integration points. It is important in this context, that the use of the Taylor assumption locally allows one to map more than one preferred crystallographic orientation on each integration point. In the second step, the mapped center orientations of the texture components are statistically rotated in such a fashion that the resulting distribution of all the rotated orientations reproduces exactly the desired texture component function. In other words the orientation scatter individually described by each texture component function according to the texture component method is mapped onto the finite element mesh by systematically modifying the orientations at each point in a way

which exactly imitates the orientation scatter of the texture component. This means that the scatter which was originally only given in orientation space is now matched by an equivalent scatter both, in real space and in orientation space. This procedure is individually conducted for all prescribed texture components extracted from initial experimental or theoretical data.

The random scattering background component can be mapped by adding to each integration point a randomly chosen orientation using the volume fraction suggested by the texture component fit so that the total set of all these orientations amounts to a random distribution with the correct volume fraction. This method is useful since during plastic deformation additional texture components can gradually build up from this random component as is known from corresponding experiments which show that the random texture portion changes during forming.

6 Example of a polycrystal plasticity simulation

In the following we present results obtained from a cup drawing simulation using a crystal plasticity finite element method in conjunction with the texture component method outlined above. Simulations of cup drawing, particularly those which predict details of the shape change, depend on details of the contact situation between sample and tool. The cup drawing simulations were conducted under the assumption that the circular blank being drawn had an initial radius of 100 mm and an initial thickness of 0.82 mm. The blank was modeled using 432 elements of type C3D8 and 80 elements of type C3D6. The interaction between the blank and the blank holder was assumed as a soft contact to impose the appropriate clamping pressure in the thickness direction of the element between blank, die, and blank holder. The simulations used an exponential soft contact function.

Figure 4 shows the simulated and experimentally observed development of earing in a cup drawn aluminium sample together with the experimental and reproduced pole figures. The diagram shows simulation results for a specimen the texture of which was approximated using a volume fraction of 29 % of an orientation close to the cube component (Euler angles at Gauss maximum: φ_1=197.87°, ϕ=6.47°, φ_2 =245.00°) and the rest (71%) as random texture background component. The texture reproduced by the component method given in terms of {111} and {200} pole figure projections shows good agreement with the original experimental data. The pole figures are shown in stereographic projections using 1.0, 2.0, 3.0, 4.0, 7.0 contour levels. The predicted distribution of the earing height reveals a very good correspondence with the simulation result.

7 Conclusions

The study discussed various reproduction methods of crystallographic orientation distributions with respect to their applicability in discrete simulation methods of integral polycrystal anisotropy properties which use the crystal orientation as an independent state variable in their underlying constitutive laws. We discussed direct pole figure inversion, Fourier-type series expansions, and the texture component method. The latter method which employs Lorentz or Gauss shaped spherical functions is well suited for the described task. It

offers a good compromise between discreteness (spherical localization), exactness (texture approximation can be achieved by a few texture components), compactness (simple functions), scalability (the number of used texture components can be varied according to the desired precision of the texture fit), and physical significance (texture components are related to microstructural mechanisms). The integration of the texture components into property simulations was demonstrated based on feeding discrete localized spherical texture components onto the Gauss points of the mesh of a finite element simulation which used a crystal plasticity constitutive law. The method was tested and the results were compared to experimental data.

8 References

[1] K. HELMING, Materials Science Forum, **157-162**, 363 (1994).

[2] R.J. ROE, Journ. apl. phys. **36**, 2024 (1965).

[3] H.J. BUNGE, Z. Metallkunde **56**, 872 (1965).

[4] H.J. BUNGE, Texture Analysis in Materials Science, Butterworths, London, England, 1982.

[5] H.-R. WENK, H.J. BUNGE, J.S. KALLEND, K. LÜCKE, S. MATTHIES, J. POSPIECH, and P. Van Houtte, Orientation distributions: Representation and determination. Summary Report from a panel discussion at the Eighth Int. Conf. on Textures of Materials, Proceedings Eighth Int. Conf. on Textures of Materials (ICOTOM 8), The Metallurgical Society of AIME., Warrendale, Pennsylvania, USA, 17 (1988).

[6] S. MATTHIES, H.-R. WENK, and G.W. VINEL, J. appl. cryst. **21**, 285 (1988).

[7] M. DAHMS and H.J. BUNGE, J. appl. cryst. **22**, 439 (1989).

[8] M. DAHMS, Textures and Microstructures **19**, 169 (1992).

[9] D. RAABE, Textures and Microstructures **23**, 115 (1995).

[10] R.D. WILLIAMS, J. appl. phys. **39**, 4329 (1968).

[11] D. RUER and R. BARO, Adv. X-ray anal. **20**, 187 (1977).

[12] J. IMHOF, Z. Metallkunde **68**, 38 (1977).

[13] S. MATTHIES and G.W. VINEL, phys. stat. sol. (b) **112**, K111-120 (1982).

[14] K. PAWLIK, phys. stat. sol. (b) **134**, 477 (1986).

[15] D. RAABE and K. LÜCKE, phys. stat. sol. (b) **180**, 59 (1993).

[16] D. RAABE and K. LÜCKE, Mater. Sc. Forum **157–162**, 413 (1994).

[17] K. LÜCKE, J. POSPIECH, J. JURA, and J. HIRSCH, Z. Metallkunde **77**, 312 (1986).

[18] K. LÜCKE, J. POSPIECH, K.H. VIRNICH, and J. JURA, Acta Metall. **29**, 167 (1981).

[19] S. MATTHIES, G.W. VINEL, and K. HELMING, Standard Distributions in Texture Analysis, Vols. I–III, Akademie Verlag, Berlin, Germany (1987–1990).

[20] K. HELMING, Texturapproximation durch Modellkomponenten (in German), Habilitation Thesis, Technical University Clausthal, Germany, Cuvillier Verlag Göttingen, Germany (1996).

[21] K. HELMING and T. ESCHNER, Cryst. Res. Technol. **25**, K203–K208 (1990).

[22] K. HELMING, R.A. SCHWARZER, B. RAUSCHENBACH, S. GEIER, B. LEISS, H.-R. WENK, K. ULLEMEIER, and J. HEINITZ, Z. Metallkunde **85**, 545 (1994).

[23] G. WASSERMANN and J. GREWEN, Texturen metallischer Werkstoffe (in German), Springer-Verlag Berlin, Germany (1969).

[24] H.J. BUNGE, Mater. Sc. Forum **273-275**, 3 (1998).

[25] D. RAABE, Z. ZHAO, and F. ROTERS, Steel Research **72**, 421 (2001).

[26] Z. ZHAO, F. ROTERS, W. MAO, D. RAABE, Adv. Eng. Materials **3**, 984 (2001).

[27] D. RAABE, Z. ZHAO, and F. ROTERS, Materials Science Forum, in press (2002).

9 Figures

Figure 1
The prediction of integral polycrystal anisotropy can be split into two quite separate tasks [1]. The first one is the formulation of a solution method which uses texture as a state variable. This is typically achieved by formulating an orientation dependent constitutive law which maps the requested physical anisotropy at the single crystal scale and by embedding this formulation into a finite element code (elasticity in the present case). The numerical implementation then tackles the interaction of the differently oriented volume portion and thereby predicts the integral response of the sample under loads. Any such formulation requires a *discrete* representation of the orientation distribution function or a portion of it at each integration point. Therefore, the second task consists in mapping *single* orientations directly on the Gauss points of the finite element mesh or in decomposing orientation distributions in such a way that they can be subsequently mapped on a mesh in a manner that they correspond to the initial overall distribution.

Figure 2
Schematical presentation of a spherical texture component c with a preferred orientation g^c and scatter width b^c. $f^c(g)$ only depends on $\tilde{\omega}^c = \tilde{\omega}(g^c, g)$, i.e. it is independent on the rotation axis $\tilde{n}^c$ [20-22].

Figure 3a
Principle of the texture component method for the calculation of the integral anisotropy of polycrystalline matter. The example in Figure 3a refers to a simulation of the integral elastic stiffness of a textured polycrystal. In this case the orientations are mapped as independent state variable on each Gauss point and the single crystal stiffness modulus acts as a constitutive law.

Figure 3b
Principle of the texture component method for the calculation of the integral anisotropy of polycrystalline matter. The example given in Figure 3b refers to a simulation of the integral elastic-plastic response and the corresponding crystallographic reorientation rates of a textured polycrystal. In this case the orientations are also mapped as independent state variable on each Gauss point and the single crystal stiffness and slip systems including some plastic hardening rule act as constitutive laws.

Figure 4
Simulation and experimental results for earing in an aluminum sample the texture of which was approximated using a volume fraction of 29 % of an orientation close to the cube component (Euler angles at Gauss maximum: φ_1=197.87°, ϕ=6.47°, φ_2 =245.00°) and the rest as random texture background component. The reproduced texture shows good agreement with the original experimental pole figure. The predicted distribution of the earing height reveals a very good correspondence with the simulation result.

Figure 1

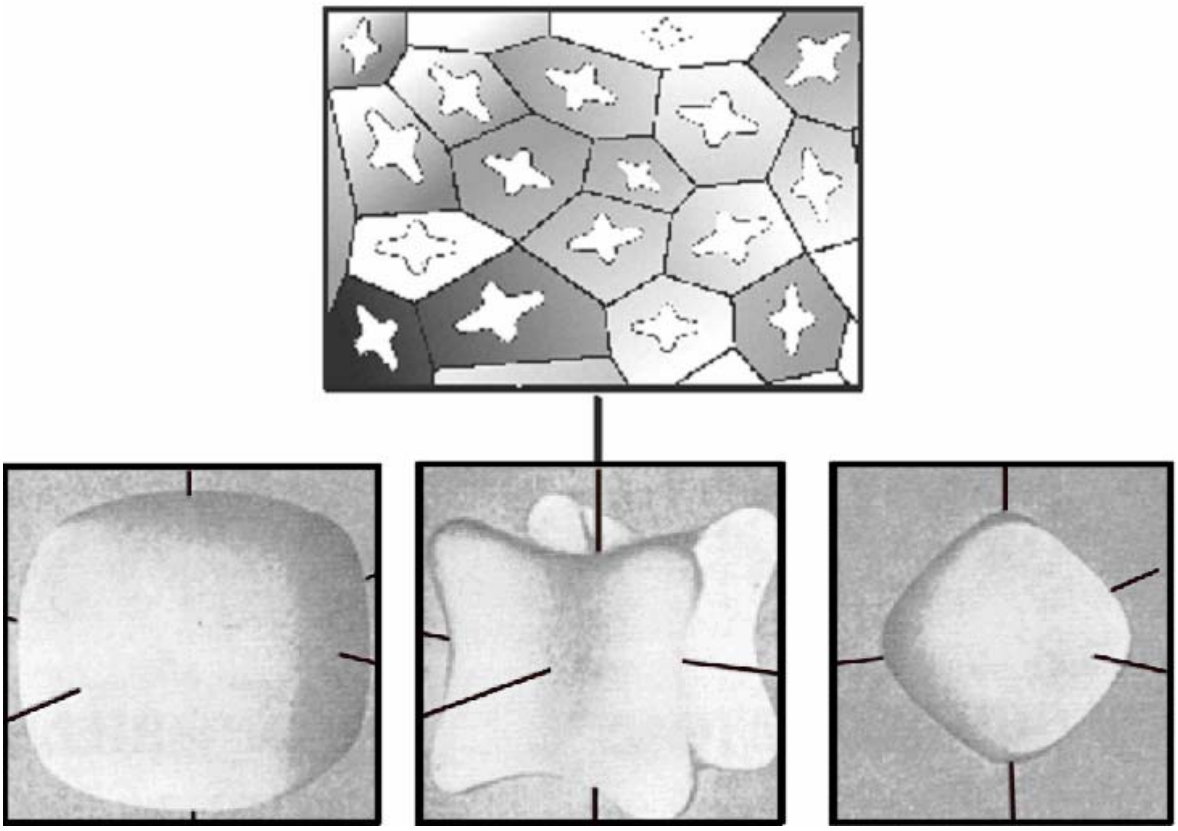

Figure 2

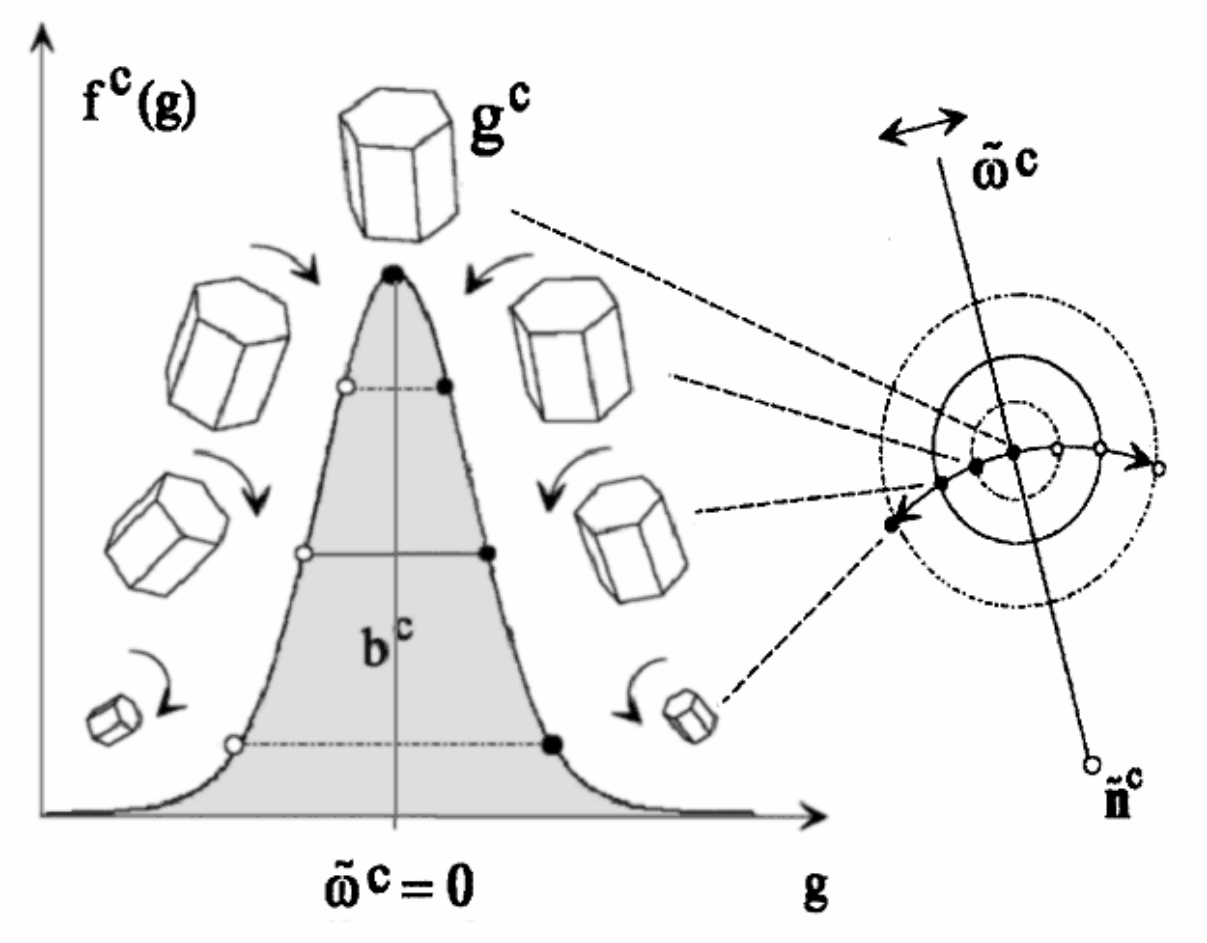

Figure 3a

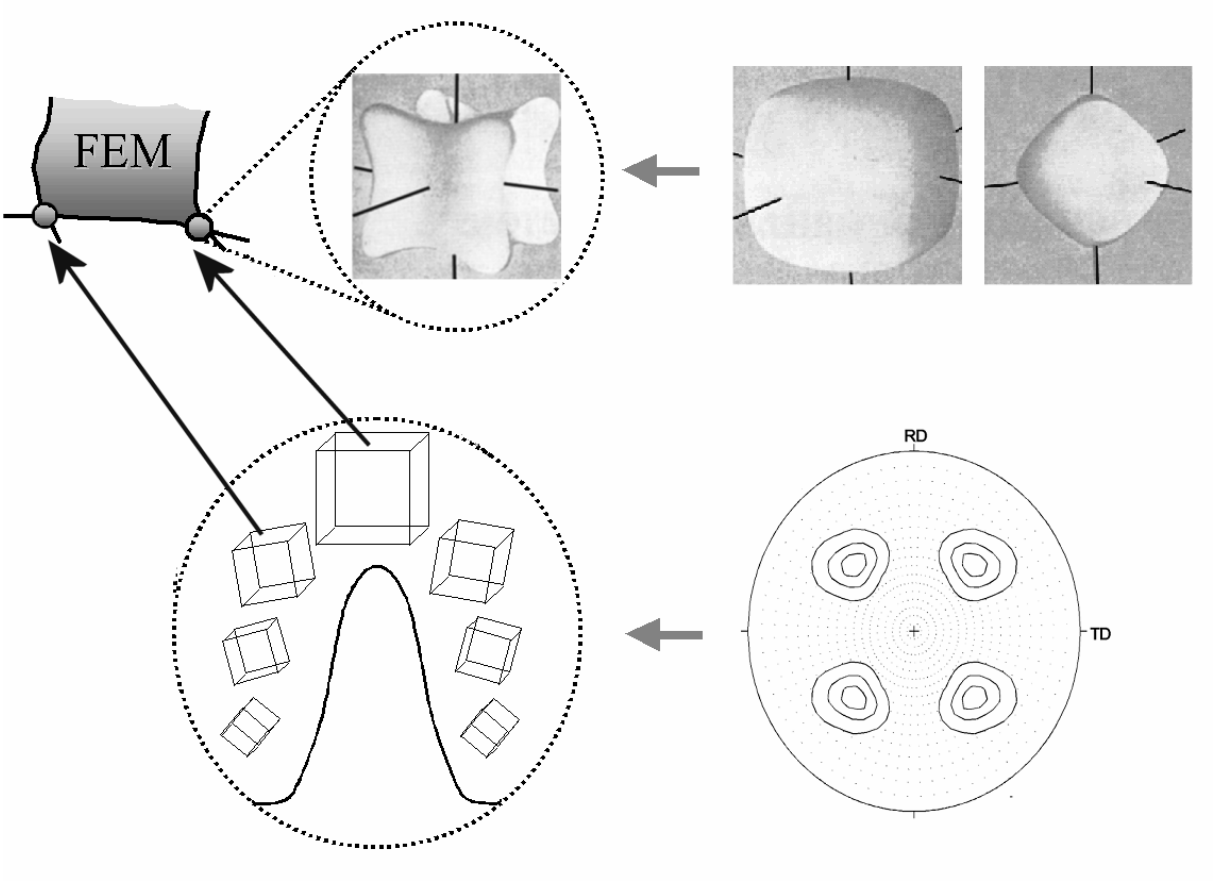

Figure 3b

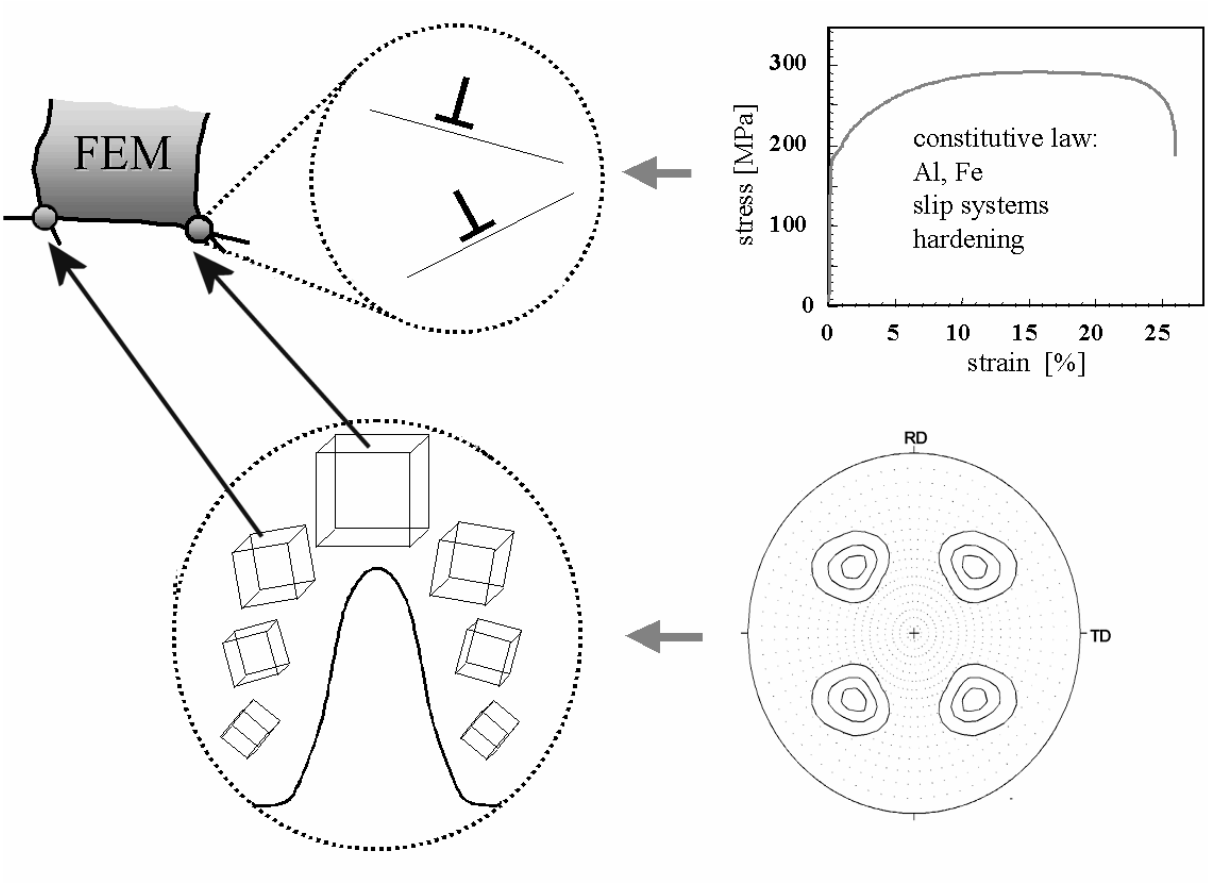
FEM
300
200
100
0
stress [MPa]
0
5
10
15
20
25
strain [%]
constitutive law:
Al, Fe
slip systems
hardening
RD
TD

Figure 4

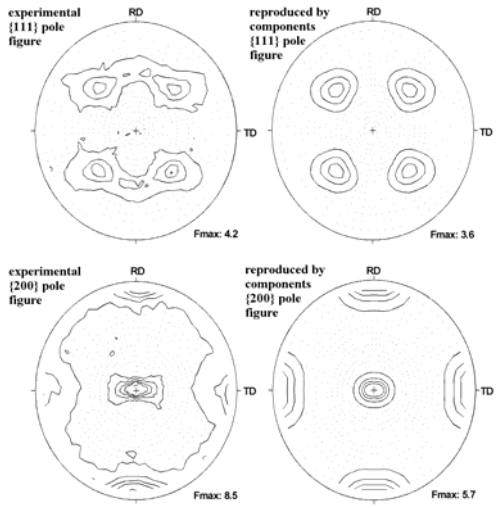
experimental {111} pole figure
RD
TD
Fmax: 4.2
reproduced by components {111} pole figure
RD
TD
Fmax: 3.6
experimental {200} pole figure
RD
TD
Fmax: 8.5
reproduced by components {200} pole figure
RD
TD
Fmax: 5.7

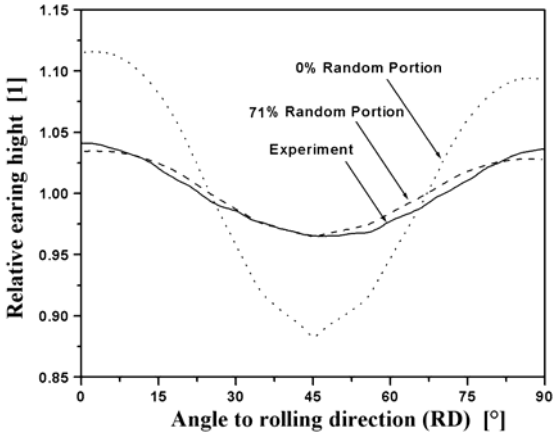
Relative earing hight [1]
1.15
1.10
1.05
1.00
0.95
0.90
0.85
0% Random Portion
71% Random Portion
Experiment
0
15
30
45
60
75
90
Angle to rolling direction (RD) [°]